Magnesium Technology 2012
Edited by: Suveen N. Mathaudhu, Wim H. Sillekens, Neale R. Neelameggham, and Norbert Hort
TMS (The Minerals, Metals & Materials Society), 2012

EFFECT OF Ca ADDITION ON THE MICROSTRUCTURAL AND MECHANICAL PROPERTIES OF AZ51/1.5Al_2O_3 MAGNESIUM NANOCOMPOSITE

Md Ershadul Alam[1], Rowshan Ara Rima[1], Abdelmagid Salem Hamouda[1], Quy Bau Nguyen[2] and Manoj Gupta[2]
[1] Department of Mechanical and Industrial Engineering, College of Engineering, Qatar University, Doha, Qatar 2713
[2] Department of Mechanical Engineering, National University of Singapore, 9 Engineering Drive 1, Singapore 117576

Keywords: Magnesium, AZ51-Al_2O_3, Ca, Nanocomposite, Mechanical properties.

Abstract

In the present study, new AZ51/1.5Al_2O_3-1Ca magnesium nanocomposite was successfully synthesized by simultaneously adding 2 wt. % aluminum, 1 wt.% Ca and 1.5 vol.% nano-sized Al_2O_3 (50 nm) into AZ31 matrix using an innovative disintegrated melt deposition technique. AZ51/1.5Al_2O_3 nanocomposite was developed following the same processing route except adding Ca. All nanocomposite samples were then subsequently hot extruded at 400 ^{0}C and characterized. Microstructural characterization studies revealed uniaxial grain size, reasonably uniform distribution of intermetallics and minimal porosity. Results also showed that the Ca addition into AZ51/Al_2O_3 nanocomposite helped to reduce the average grain size. Physical properties characterization revealed that addition of Ca reduced the coefficient of thermal expansion when compared to Ca free nanocomposite. The presence of Ca also assisted in improving overall mechanical properties including microhardness, 0.2% yield strength and ultimate tensile strength while the ductility was compromised.

Introduction

Magnesium based materials, with a density around 1.74 g/cm^3, are the lightest engineering materials available in the earth which is about two-thirds of the density of aluminum based (~ 2.70 g/cm^3) and one-quarter of that of ferrous based (~ 7.87 g/cm^3) materials [1]. Therefore, magnesium based alloys are attracting much attention as light weight materials due to the increasing demand for the reduction of fuel consumption and green house gas (CO_2) emission [2-3]. Hence, its use is gaining significance in certain key engineering applications, particularly in automobile, aviation, electronics and consumer industries where weight is one of the most important criteria in the choice of materials [2-7].

Magnesium alloys that contain aluminum (Al) and zinc (Zn) are known as AZ alloys [8-10]. These alloys are easily available, reasonably priced and used in many engineering applications. However, the properties of these alloys can be further improved by applying metal matrix composites (MMCs) technique. This is particularly useful in engineering applications especially when properties of traditional materials like metals, polymers and ceramics are not able to match with expected properties. In recent studies, it has been observed that the addition of nano-sized reinforcements such as ceramic oxides, SiC and carbon nanotubes can lead to a simultaneous increase in strength and ductility of magnesium [11-13]. Among all the reinforcements, it can be observed from the study that the 1.5 vol. % addition of nano-sized alumina particulates in magnesium based matrix showed the best overall combination of microstructural and mechanical properties [11]. Accordingly, AZ51/1.5 vol. % Al_2O_3 nanocomposite was developed. Results of literature search also indicate that the addition of Ca assists in grain refinement and enhancing corrosion resistance as well as thermal and mechanical properties of magnesium based alloys and their composites [8-10, 14-15]. Literature search results also indicate that no attempt has been made so far to synthesize and characterize AZ51/Al_2O_3-Ca nanocomposite. Accordingly, in the present study, new AZ51/1.5 Al_2O_3-1Ca nanocomposite has been synthesized using disintegrated melt deposition technique.

Characterization studies were carried out on these formulations to investigate their physical, microstructural and mechanical properties. These include density and porosity measurements, the coefficient of thermal expansion, grain morphology, x-ray diffraction analysis, optical and scanning electron microscopy, microhardness, tensile tests and fractography studies.

Experimental Procedures

Materials

In the present study, AZ31 magnesium alloy ingots (2.94% Al, 0.87% Zn, 0.57% Mn, 0.0027% Fe, 0.0112% Si, 0.0008% Cu, 0.0005% Ni and balance Mg, supplied by Tokyo Magnesium Company Limited, Japan) were used as a matrix material and cut into small pieces so that they can be placed into the graphite crucible easily. The aluminum lumps of 99.5% purity (supplied by Alfa Aesar, USA) and the reinforcement in the form of 50 nm alumina powder of 99.4 % purity (supplied by Baikowski, Japan) were used for developing AZ51/1.5Al_2O_3 nanocomposite. Ca granules of 99.6% purity (supplied by Alfa Aesar, USA) were also used with AZ31, Al and nano-sized Al_2O_3 to develop AZ51/1.5Al_2O_3-1Ca nanocomposite.

Primary Processing

Synthesis of AZ51/1.5Al_2O_3 and AZ51/1.5Al_2O_3-1Ca magnesium based nanocomposites was carried out using disintegrated melt deposition (DMD) technique. Synthesis of AZ51/1.5 Al_2O_3-1Ca nanocomposite involved heating the AZ31 magnesium alloy pieces with the addition of 2 wt.% Al, 1 wt.% Ca and 1.5 vol. % (~3.3 wt.%) nano-sized Al_2O_3 to 750 ^{0}C in an inert Ar gas atmosphere in a graphite crucible using a resistance heating furnace. The crucible was equipped with an arrangement for bottom pouring. Upon reaching the superheat temperature, the molten slurry was stirred for 5 min at 450 rev./min using a twin blade (pitch 45^0) mild steel impeller to facilitate the incorporation and uniform distribution of reinforcement particulates in the metallic matrix. The impeller was coated with Zirtex 25 (86% ZrO_2, 8.8% Y_2O_3, 3.6% SiO_2, 1.2% K_2O and Na_2O, and 0.3% trace inorganic) to avoid iron contamination of the molten metal. The melt was then released through a 10-mm diameter orifice at the base of the crucible. The melt material was disintegrated by two jets of argon gas orientated normal to the melt stream. The argon gas flow rate was maintained at 25 L /min. The

disintegrated melt slurry was subsequently deposited onto a metallic substrate. Preform of 40-mm diameter was obtained following the deposition stage. The synthesis of AZ51/1.5Al_2O_3 magnesium nanocomposite was carried out using steps similar to those employed for AZ51/1.5Al_2O_3-1Ca except that no Ca were added (see Table I).

Table I. Compositions of Synthesized Nanocomposites

Compositions	Al (Wt. %)	n- Al_2O_3 (Vol. %)	Ca (Wt. %)	AZ31
AZ51/Al_2O_3	2	1.5	-	Balance
AZ51/Al_2O_3-Ca	2	1.5	1	Balance

Secondary Processing

Pre-Extrusion: The 40 mm diameter ingots were machined down using a lathe machine to a diameter of 36 mm and cut into billets with heights of approximately 45 mm. They were then lathed in the direction perpendicular to the length of the ingot to ensure both ends are flat and perpendicular to the surface. The billets were then sprayed with colloidal graphite for lubrication purposes.

Extrusion: The billets were first soaked at 400 ^{0}C for 60 minutes in a constant temperature furnace before extrusion. Extrusion was performed on a 150 tonne hydraulic press using an extrusion ratio of 20.25:1, producing rods of 8 mm diameter.

Post-Extrusion: After extrusion, the extruded rods were machined to produce tensile specimens. Sections of approximately 4 to 10 mm in height were also cut by a low speed diamond blade and the surface graphite was then cleaned-off to use for various characterization studies.

Density and Porosity Measurements

Density (ρ) measurements were performed in accordance with Archimedes' principle on three randomly selected polished samples of AZ51/Al_2O_3 and AZ51/Al_2O_3-Ca nanocomposites taken from the extruded rods. Distilled water was used as the immersion fluid. The samples were weighed using an A&D ER-182A electronic balance; with an accuracy of ±0.0001 g. Theoretical densities of materials were calculated assuming they are fully-dense. Rule-of-Mixture was used in all calculations. The porosity was calculated by using the theoretical and experimental densities.

Microstructural Characterization

Microstructural characterization studies were conducted on metallographically polished extruded samples to investigate morphological characteristics of grains, reinforcement distribution and interfacial integrity between the matrix and reinforcement. The etching solution (5 ml acetic acid, 6 g picric acid, 10 ml water and 100 ml ethanol) was applied for approximately 10 seconds using a swabbing technique and then washed under running water to reveal the grain boundaries [16-17]. The sample was then analyzed using the Olympus BH2-UMA metallographic optical microscope equipped with Olympus DP-10 microscope digital camera. The grain boundaries were then traced out from the micrographs with the aid of the Adobe Photoshop program. Image analysis using the Scion system was carried out to determine the grain size of the materials.

The presence and distribution of the intermetallic phase was investigated using the JEOL JSM-5600LV Scanning Electron Microscope (SEM) and Hitachi S-4300 FESEM. Polished specimens were observed at 1000x magnification to reveal the intermetallic phase.

X-Ray Diffraction Studies

X-ray diffraction analysis was conducted using the automated Shimadzu LAB-X XRD-6000 x-ray diffractometer. Flat, ground and ultrasonically cleaned specimens of approximately 5 mm in height were exposed to CuK_α radiation (λ = 1.54056 Å) with a scanning speed of 2 ^{0}/min. The scanning range was 30^0 to 80^0 for all samples. A plot of intensity against 2θ (θ represents Bragg angle) was obtained, illustrating peaks at different Bragg angles. The Bragg angles corresponding to different peaks were noted; and the values of interplanar spacing (d-spacing) obtained from the computerized output were compared with the standard values from the International Centre for Diffraction Data's Powder Diffraction File (PDF).

Coefficient of Thermal Expansion

The coefficients of thermal expansion (CTE) of all the compositions were determined by measuring the displacement of the samples as a function of temperature in the temperature range of 50 ^{0}C- 400 ^{0}C using an automated SETARAM 92-16/18 thermo-mechanical analyzer.

Mechanical Characteristics

The mechanical properties carried out on all samples were investigated by conducting tensile and microhardness tests. All experiments were carried out at room temperature.

Microhardness Test: The microhardness tests were conducted on flat and metallographically polished specimens. The test was conducted using a Shimadzu HMV automatic digital microhardness tester with a Vickers indenter (square-based pyramidal-shaped diamond indenter with face angle of 136 ^{0}). An indenting load of 25 gf and a dwell time of 15 seconds were used. Testing was performed in accordance with ASTM test standard E384-08. Indentations were performed on the matrix and measurements were recorded in Vickers Hardness (HV).

Tensile Testing: The tensile properties of each sample were determined in accordance with ASTM test standard E8M-08. Round tension test specimens of 5 mm in diameter were machined from the 8 mm extruded rod. An average of five tensile specimens could be obtained from a single rod, and a minimum of four tensile tests were conducted for each sample. Tests were performed on the 810 Material Test System (MTS) with an extensometer of 25 mm gauge length and a crosshead speed of 0.254 mm/min was used. The raw stress-strain data recorded was extracted to be analyzed. Broken test specimens were labeled individually, carefully handled and packed into individual plastic bags to prevent damage of the fractured surface. A Microsoft Excel program was written to analyze the raw data extracted. Then, 0.2% offset yield strength (0.2% YS), ultimate tensile

strength (UTS) and failure strain was computed via a series of Microsoft Excel functions.

Fracture Behavior: The fracture surfaces of the broken tensile samples were analyzed to investigate the failure mechanisms that occurred during the tensile tests. Fractography studies were performed on the JEOL JSM-5600LV Scanning Electron Microscope and Hitachi S-4300 FESEM. Images were captured at an accelerating voltage of 15 kV and a working distance of about 16 mm. Macromechanism of these fracture surfaces were also investigated.

Results

Macrostructure

The result of macrostructural characterization conducted on the as deposited AZ51/Al_2O_3 and AZ51/Al_2O_3-Ca nanocomposites did not reveal any presence of macropores, shrinkage, cracks or any other defects. Following extrusion, there was also no evidence of any macrostructural defects.

Density and Porosity Measurements

The results of the density measurements are shown in Table II. Results show that near dense nanocomposites can be developed using the fabrication methodology adopted in the present study. Results also revealed that all nanocomposite samples exhibited minimal porosity.

Table II. Results of Density and Porosity Measurements

Compositions	Density (g/cm^3)		Porosity (%)
	Theo.	Expt.	
AZ51/Al_2O_3	1.827	1.825	0.09
AZ51/Al_2O_3-Ca	1.824	1.822	0.12

Microstructural Characteristics

Microstructural studies conducted on the extruded specimens showed near equiaxed grain morphology (see Table III and Figure 1). Average grain size of AZ51/Al_2O_3 nanocomposite samples decreased with the addition of Ca.

Table III. Results of Grain Morphology

Compositions	Grain Size (μm)	Aspect Ratio	Roundness[1]
AZ51/Al_2O_3	3.6 ± 1.5	1.7 ± 0.5	1.6 ± 0.4
AZ51/Al_2O_3-Ca	1.7 ± 0.5	1.6 ± 0.3	1.6 ± 0.4

1. Roundness is the shape of the grain expressed by the formula (perimeter)^2 / 4π (area)

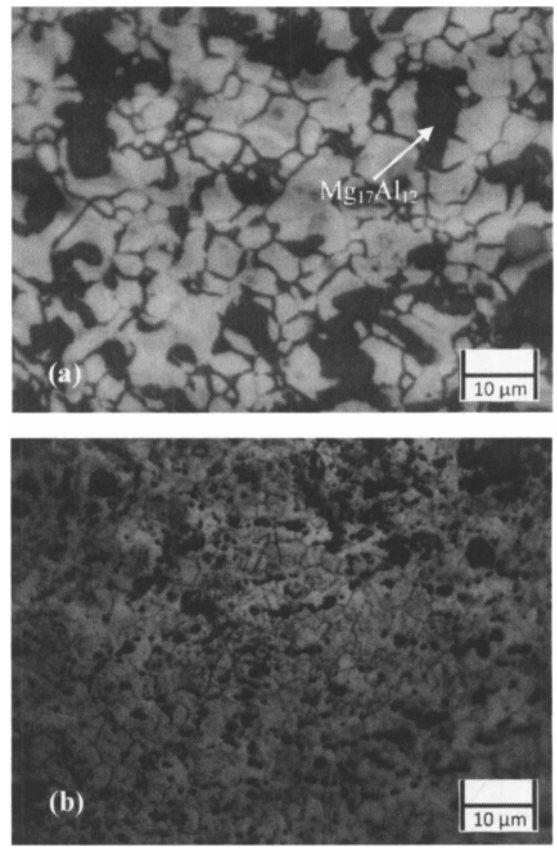

Figure 1. Representative optical micrographs showing the grain morphology (1000x) of: (a) AZ51/Al_2O_3 and (b) AZ51/Al_2O_3-Ca samples, respectively.

Microstructural characterization studies were also conducted on the extruded and polished samples to observe the shape and distribution of intermetallic phases (see Figure 2). The white color second phase corresponds to $Mg_{17}Al_{12}$ and the light gray color phase corresponds to (Mg, Al)$_2$Ca phase based on previous study conducted by the same research group (see Figure 2b) [10]. Results showed that amount of $Mg_{17}Al_{12}$ phase decreased noticeably with the addition of Ca into AZ51/Al_2O_3 nanocomposite (see Figures 2 (a) and (b)).Figure 2(c) showed the interfacial bonding between the (Mg, Al)$_2$Ca and the matrix.

X-Ray Diffraction

X-ray diffraction (XRD) was carried out on all extruded samples. The obtained lattice spacing's (d-spacing) and two-theta (2θ) value were compared with the standard values for magnesium and the Mg-Al-Ca intermetallic phases. Results showed the presence of eutectic $Al_{12}Mg_{17}$ intermetallic phase in the α-Mg phase for the case of AZ51/Al_2O_3 samples while both $Mg_{17}Al_{12}$ and (Mg, Al)$_2$Ca intermetallic phases were found in the α-Mg matrix for the case of AZ51/Al_2O_3-Ca sample. However, no nano-sized alumina phase was detected from the XRD analysis.

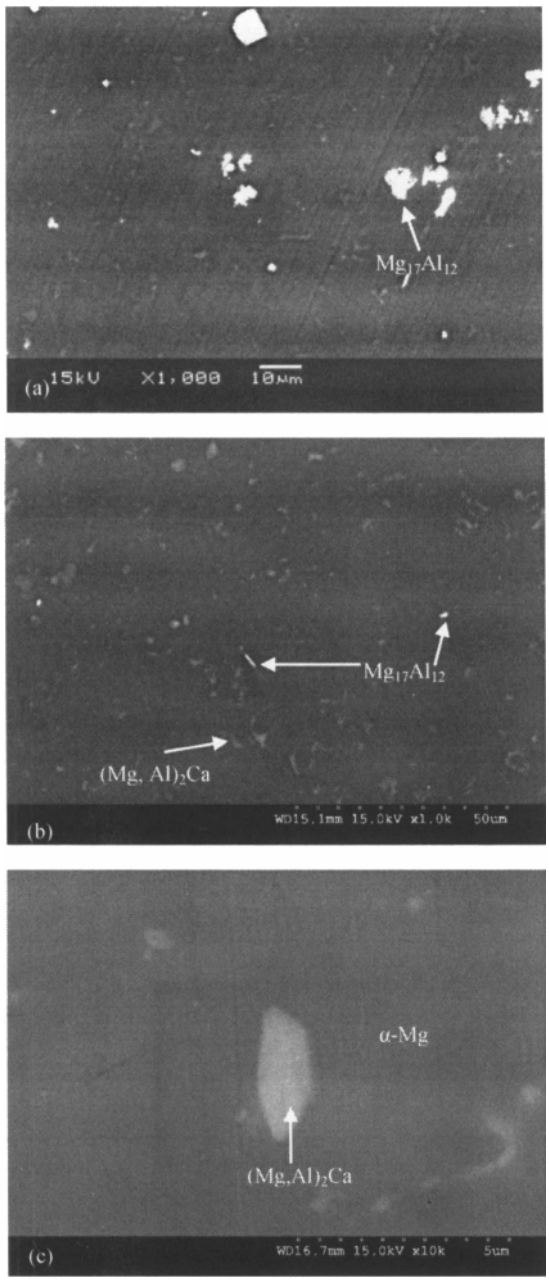

Figure 2. Representative SEM and FESEM micrographs showing the shape and distribution of $Mg_{17}Al_{12}$ and $(Mg, Al)_2Ca$ phases in the case of: (a) $AZ51/Al_2O_3$ and (b) $AZ51/Al_2O_3$-Ca samples, respectively. Figure (c) shows the interfacial bonding between second phase and the matrix.

Coefficient of Thermal Expansion

Table IV shows the results of coefficient of thermal expansion measurements obtained from $AZ51/Al_2O_3$ and $AZ51/Al_2O_3$-Ca samples. The results revealed a reduction in CTE of the $AZ51/Al_2O_3$ nanocomposite with the addition of Ca. This value is much lower than that of AZ31 sample.

Table IV. Results of CTE and Microhardness Tests

Compositions	CTE (μm/mK)	Microhardness (HV)
$AZ51/Al_2O_3$	26.2	110 ± 3
$AZ51/Al_2O_3$-Ca	25.7	119 ± 5
AZ31[16]	28.8	66 ± 2
AZ61A [1]	-	62

Mechanical Characteristics

Microhardness Test: Vickers microhardness tests were conducted on all extruded and polished samples (see Table IV). Results revealed that the addition of Ca increased the microhardness value of $AZ51/Al_2O_3$ nanocomposite. More than 8% microhardness value was increased when 1 wt. % Ca was added into $AZ51/Al_2O_3$ nanocomposite. Moreover, $AZ51/Al_2O_3$-Ca magnesium based nanocomposite exhibited 80% and 92% higher hardness when compared to AZ31 and commercially available AZ61A alloy, respectively (see Table IV).

Tensile Test: Results of ambient temperature tensile test on round tensile specimens revealed that the addition of Ca in $AZ51/Al_2O_3$ nanocomposite increased the 0.2% yield strength (YS) and ultimate tensile strength (UTS) (see Table V). $AZ51/Al_2O_3$-Ca nanocomposite exhibited around 7% and 2% higher YS and UTS, respectively, when compared to $AZ51/Al_2O_3$ samples. Results also showed that the Ca added nanocomposite exhibited 25% and 16% higher 0.2% YS and UTS, respectively, when compared to the AZ31 alloy. However, failure strain (FS) dropped with the addition of Ca.

Table V. Results of Room Temperature Tensile Properties

Compositions	0.2 % YS (MPa)	UTS (MPa)	FS (%)
$AZ51/Al_2O_3$	211 ± 4	311 ± 3	13.4 ± 1.2
$AZ51/Al_2O_3$-Ca	225 ± 3	317 ± 4	9.4 ± 0.5
AZ31[16]	180 ± 3	273 ± 6	10.6 ± 1.3

Fracture Behavior: Macroscopic fracture characteristics of the broken tensile samples revealed that all samples exhibited shear-type ductile fracture mode. Microscopic features of fracture surface were also conducted on the tensile fractured surface using SEM/FESEM and dimple-like features were observed in all the cases.

Discussion

Macrostructure

Syntheses of $AZ51/Al_2O_3$ and $AZ51/Al_2O_3$-Ca nanocomposites were successfully accomplished by using DMD technique

followed by hot extrusion. Observations made during DMD processing revealed: (a) minimal oxidation of melts, (b) undetectable reaction between graphite crucible and melts and (c) absence of blowholes and macropores. The results suggest the appropriateness of processing parameters and methodology used in the present study. These observations are also consistent with the previous findings made on DMD processed magnesium based materials [10-11, 16].

Density and Porosity Measurements

The experimental density obtained by the Archimedes' principle exhibited that the density of newly developed magnesium based AZ51/Al_2O_3-Ca nanocomposite slightly decreased with the addition of elemental Ca into AZ51/Al_2O_3 (see Table II). This can be attributed to the relatively lower dense Ca (1.55 g/cm^3) addition into AZ31 matrix (1.78 g/cm^3) [1, 11]. Obtained results also revealed that the experimental values were relatively close to the theoretical values. This indicated that the experimental method used was accurate, and the experimental density of the fabricated materials could be calculated.

Porosity of the materials was calculated using the theoretical and the experimental densities obtained from each sample. The highest porosity obtained among the samples was 0.12% (see Table II), hence indicating that near dense materials was obtained and that the alloying and reinforcing constituents were successfully incorporated into the matrix. Therefore, as demonstrated by prior studies, the fabrication route of DMD followed by hot extrusion is capable of producing new AZ51/Al_2O_3-Ca nanocomposite with minimal porosity [11].

Microstructural Characteristics

The results of microstructural characterization revealed the presence of nearly equiaxed grains (see Table III and Figure 1) in Ca-added and Ca-free AZ51/Al_2O_3 nanocomposite samples. Second phases predominantly located at grain boundaries were observed in all samples (see Figure 1). Addition of elemental Ca into AZ51/Al_2O_3 decreased the average grain size (see Table III and Figure 1). This can be attributed to the pinning of grain boundaries by the higher amount of (Mg, Al)$_2$Ca second phases resulting in limited grain growth.

SEM and FESEM micrographs of the etched samples revealed the presence and good distribution of the equilibrium intermetallic phases $Mg_{17}Al_{12}$ and (Mg, Al)$_2$Ca (see Figure 2). This could be attributed to the use of a layered arrangement for the raw materials during the solidification process and effective stirring parameters. The successful disintegration of the melt and the inert atmosphere caused by the argon gas jets were also the contributing factors. In the AZ51/Al_2O_3 system, only $Mg_{17}Al_{12}$ intermetallic was found while for the AZ51/Al_2O_3-Ca system, both $Mg_{17}Al_{12}$ and (Mg,Al)$_2$Ca intermetallics were observed (see Figure 2). Amount of $Mg_{17}Al_{12}$ decreased with the addition of Ca. This can be attributed to the formation of (Mg, Al)$_2$Ca phase where Al reacted with Ca. Figure 2(c) revealed the strong interfacial bonding between matrix and second phase.

X-Ray Diffraction

X-Ray diffraction results confirmed the presence of the intermetallic phase $Mg_{17}Al_{12}$ in AZ51/Al_2O_3 nanocomposite while both $Mg_{17}Al_{12}$ and (Mg, Al)$_2$Ca phases were observed for AZ51/Al_2O_3-Ca samples. However, the presence of the nano-sized alumina was not identified. This can be attributed to the limitation of the filtered x-ray to detect phases with less than 2 vol.% of nano-sized particles [16, 18].

Coefficient of Thermal Expansion

The results of CTE measurement showed that the addition of Ca alloying constituent into AZ51/Al_2O_3 nanocomposite decreases the average CTE values of the material (see Table IV). The results suggested an appropriate integration of AZ51/Al_2O_3composite with elemental Ca leading to low CTE values. Moreover, the lower CTE values of Ca (22.3 μm/mK) than Mg (25.2 μm/mK) also helped to lower the average CTE value of the newly developed compositions [1, 16].

Mechanical Characteristics

Microhardness Test: The experimental results of microhardness measurement are shown in Table IV. Significant increase in microhardness was observed in AZ51/Al_2O_3-Ca composite samples when compared to AZ51/Al_2O_3 nanocomposite, pure AZ31 and commercially available AZ61A samples (see Table IV). This can be attributed to the lower average grain size of the new compositions when compared to AZ51/Al_2O_3 which is associated with larger grain boundary area leading to higher hardness [16, 19]. The increase in hardness can be attributed to: (i) the solid solution hardening, (ii) the reasonably uniform distribution of harder (Mg, Al)$_2$Ca intermetallic in the matrix and (iii) higher constraint to the localized matrix deformation during indentation due to the higher presence of intermetallic [10, 16].

Tensile Test: Room temperature tensile test results revealed that the addition of elemental Ca increased the strength of AZ51/Al_2O_3 composite (see Table V and Figure 3). Tensile results also showed that the AZ51/Al_2O_3-Ca nanocomposite exhibited around 25% and 16% higher 0.2% YS and UTS, respectively, when compared to the AZ31 alloy. This can be attributed to the lower average grain size of AZ51/Al_2O_3-Ca samples when compared to AZ51/Al_2O_3 samples (see Table III and Figure 1). Presence of additional Ca modified the microstructural features, hence increasing strength. This observation is similar with the findings of other researchers obtained from AZ31B/Al_2O_3-Ca samples [10].

Failure strain decreased with Ca addition into AZ51/Al_2O_3 composite. This can be attributed to the formation and presence of sharp edge intermetallic particles which might act as a stress concentration sites (see Figure 2).

Fracture Behavior:

Macroscopic observations performed on the broken tensile samples revealed shear type fracture characteristics. Microscopic observations showed that dimple like features were predominately present in all compositions, indicating high plastic deformation (see Figure 3). However, presence of microcracks and cleavage step on the fracture surface were observed for new system, hence are responsible for the decrease in failure strain of these composites.

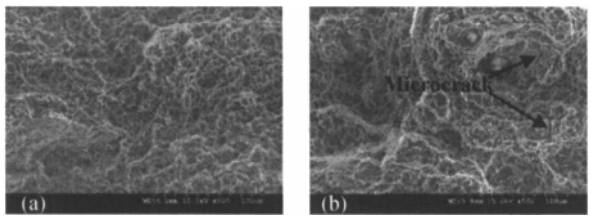

Figure 3. Representative FESEM fractographs showing the dimple like features and microcrack for: (a) AZ51/Al_2O_3 and (b) AZ51/Al_2O_3-Ca samples, respectively.

Conclusions

The following conclusions can be made from the present study:

1. AZ51/Al_2O_3 and AZ51/Al_2O_3-Ca nanocomposites can be successfully synthesized by using the disintegrated melt deposition technique followed by hot extrusion with minimal porosity.

2. The addition of Ca leads to decrease in $Mg_{17}Al_{12}$.secondary phase and form $(Mg,Al)_2Ca$ phase. Ca addition also helps to decrease average grain size. The coefficient of thermal expansion of AZ51/Al_2O_3 magnesium nanocomposite also decreases with the addition of Ca.

3. A good combination mechanical properties (in terms of microhardness, 0.2% YS and UTS) was observed for AZ51/Al_2O_3-Ca samples when compared to AZ51/Al_2O_3 samples.

Acknowledgments

The authors gratefully acknowledge the support received for this research work ref: NPRP 08-424-2-171 from the Qatar National Research Fund (QNRF), Qatar.

References

[1] J. R. Davis, "Properties and Selection: Nonferrous Alloys and Special-Purpose Materials", Formerly Tenth Edition, (ASM Handbook, Volume 2, ASM, Metal Park, Ohio, 1993) 480-515, 1099-1100, 1105-1107,1118-1128,1199, 1132-1135.

[2] S. F. Hassan and M. Gupta, "Development of Nano-Y_2O_3 Containing Magnesium Nanocomposites Using Solidification Processing", Journal of Alloys and Compounds, 429 (1-2) (2007) 176-183.

[3] R. Fink, in: K. U. Kainer (Ed.), "Die-Casting Magnesium, Magnesium Alloys and Technologies", (Wiley-VCH Verlag GmbH and Co., Germany, 2003) 23-44.

[4] B. L. Mordike and K. U. Kainer, "Magnesium Alloys and Their Applications", (Werkstoff-Informationsgesellschaft, Frankfurt, Germany, 1998).

[5] B. L. Mordike and T. Ebert, "Magnesium: Properties-Applications-Potentials", Mater. Sci. Eng. A, 302 (2001) 137-45.

[6] D. J. Lloyd, "Particle Reinforced Aluminium and Magnesium Matrix Composites", Int. Mater. Rev., 39 (1994) 1-23.

[7] F. Moll and K. U. Kainer, "Magnesium Alloys and Technology", Kainer, K. U. (Ed), (Weinheim: Wiley-VCH, Germany, (2002) 197-217.

[8] G. Wu, Y. Fan, H. Gao, C. Zhai, and Y. P. Zhu,. "The Effect of Ca and Rare Earth Elements on the Microstructure, Mechanical Properties and Corrosion Behavior of AZ91D", Mater. Sci. Eng. A, 408 (2005) 255–263.

[9] B. Jing, S. Yangshan, X. Shan, X. Feng, and Z. Tianbai, "Microstructure and Tensile Creep Behavior of Mg–4Al Based Magnesium Alloys with Alkaline Elements Sr and Ca Additions", Mater. Sci. Eng. A, 419(2006) 181–188.

[10] Q. B. Nguyen and M. Gupta, "Microstructure and Mechanical Characteristics of AZ31B/Al_2O_3 Nano-Composite with Addition of Ca", Journal of Composite Materials, 43 (2009) 5-17.

[11] Q. B. Nguyen and M. Gupta, "Increasing Significantly the Failure Strain and Work of Fracture of Solidification Processed AZ31B Using Nano-Al_2O_3 Particulates", J. Alloys Comp., 459 (2008) 244-250.

[12] C. S. Goh, J. Wei, L. C. Lee and M. Gupta, "Development of Novel Carbon Nanotube Reinforced Magnesium Nanocomposites Using the Powder Metallurgy Technique", Nanotechnology, 17 (2006) 7-12.

[13] S. F. Hassan and M. Gupta, "Effect of Different Types of Nano-Size Oxide Particulates on Microstructural and Mechanical Properties of Elemental Mg", J. Mater. Sci., 41 (2006) 2229-2236.

[14] D. Wenwen, Z. Yangshan, M. Xuegang, X. Feng, Z. Min, and W. Dengyun, "Microstructure and Mechanical Properties of Mg–Al Based Alloy with Calcium and Rare Earth Additions," Mater. Sci. Eng A, 356 (2003) 1–7.

[15] G. Y. Yuan, Z. L. Liu, Q. D. Wang, and W. J. Ding, "Microstructure Refinement of Mg–Al–Zn–Si Alloys", Materials Letters, 56 (2002) 53–58.

[16] M. E. Alam, S. Han, A. M. S. Hamouda, Q. B. Nguyen and M. Gupta, "Development of New Magnesium Based Alloys and Their Nanocomposites", Journal of Alloys and Compounds, 509 (2011) 8522-8529.

[17] A. Jager, P. Lukac, V. Gartnerova, J. Haloda, and M. Dopita, "Influence of Annealing on the Microstructure of Commercial Mg Alloy AZ31 after Mechanical Forming", Mater. Sci. Eng. A, 432 (2006) 20-25.

[18] B. D. Cullity, "Elements of X-Ray Diffraction", (3rd ed., Prentice Hall, London, 2001).

[19] G. E. Dieter, "Mechanical Metallurgy", (2nd Edition, McGraw-Hill, Inc., USA, 1976) 191-193.